Advances in Environmental Research, Vol. 1, No. 4 (2012) 289-304
DOI: http://dx.doi.org/10.12989/aer.2012.1.4.289

Performance assessment of {tris (2-methyl-1-aziridinyl) phosphine oxide} photocatalytic mineralization in a falling film reactor, using response surface methodology

J. Saien*[1], A. Raeisi[1], A.R. Soleymani[2] and M. Norouzi[1]

[1]*Department of Applied Chemistry, Bu-Ali Sina University, Hamedan 65174, Iran*
[2]*Department of Applied Chemistry, Malayer University, Malayer 65719, Iran*

(Received June 30, 2012, Revised November 30, 2012, Accepted December 12, 2012)

Abstract. Tris (2-methyl-1-aziridinyl) phosphine oxide (MAPO) is extremely poisonous and persistent in aqueous media. An efficient UV/nanoTiO_2 process was employed for its mineralization in a high duty falling film photo-reactor based on an experimental design scheme that considers interactions between the main variables. The influencing variables and their range were determined with preliminary studies. The results show substrate mineralization to some extent under mild conditions of: T = 30˚C, pH = 8.5, $[MAPO]_0$ = 60 mg L^{-1} and $[TiO_2]$ =110 mg L^{-1}. The relative importance of the influencing parameters were initial pH > temperature > $[MAPO]_0$ > $[TiO_2]$; while the interdependence of all the parameters was significant. Accordingly, a reduced quadratic expression was developed. Meanwhile, mineralization kinetic studies, based on chemical oxygen demand, revealed a power law model with order of 2.6 during process time until 150 min.

Keywords: MAPO; photocatalysis; nanoparticle; falling film reactor; response surface methodology; kinetic

1. Introduction

The activities to protect the environment include processes for waste treatment or new products development with less harmful effects (Parsa and Abbasi 2010). In recent years, various technologies have been developed for environmental remediation. Generally, the pollutants treatment is being performed by adsorption, membrane, coagulation–flocculation, oxidation–ozonation and advanced oxidation processes (AOPs). AOPs involve the generation of hydroxyl radical ($^{\bullet}OH$) that is a reactive agent and has a high oxidation potential (Ahmadi *et al*. 2005). AOPs such as UV/H_2O_2 process, Fenton and photo-Fenton catalytic reactions and TiO_2 mediated photocatalysis have been widely used to destroy organic pollutants (Karba *et al*. 2004, Thiruvenkatachari *et al*. 2008). Among these methods, photocatalysis has become a hot topic, because it can completely degrade the organic pollutants into harmless inorganic substances such as CO_2 and H_2O under moderate conditions and it does not produce hazardous byproducts. TiO_2 is one of the suitable semiconductors for photocatalysis and has been applied in various

*Corresponding author, Professor, E-mail: saien@basu.ac.ir

photocatalytic reactions because of: (i) the process occurs around ambient pressure and temperature; (ii) it has low cost and high turnover rates; and (iii) the process offers great potential as an industrial technology to detoxify wastewater (Saien and Soleymani 2007).

Several operational factors such as catalyst dosage, pH, temperature and the pollutant loading can affect the photocatalytic process behavior; therefore, optimization of these should be considered as an important step. Most of the studies dealing with optimization make use of the traditional one-factor-at-a-time approach, which is time-consuming and requires a considerable amount of reagents. A promising alternative approach is chemometric method such as response surface methodology (RSM), based on statistical design of experiments (DOEs). Chemometric experimental design in photocatalytic processes plays a crucial role in the ability of reaching the optimum of the catalytic reaction. Such statistical analyses are more efficient since they estimate interaction effects between the studied variables and determine accurately the combination of levels that produces the optimum of the processes (Sakkas and Islam 2010).

In this work, for the first time, tris (2-methyl-1-aziridinyl) phosphine oxide (MAPO) was used as a target pollutant in aqueous solutions. This compound, with aziridine groups in its structure, is water soluble and extremely poisonous (Gembitskii *et al*. 1966). It is readily absorbed by skin and produces blisters and rashes (Jonse 1944). Compounds having aziridine groups are most widely used in the textile and alkylating agents. They readily react with most compounds that form natural and synthetic fibers and papers. In this regard, when amino-groups are introduced into other compounds, their properties such as resistance against wet conditions and ability to fix dyes are improved (Gembitskii *et al*. 1966).

Here photocatalytic process was performed in a novel circulating falling film photo-reactor. In design of experiments, the operational parameters of nano TiO_2 photocatalyst dosage, initial pH, temperature and substrate initial concentration are considered as variables while the mineralization efficiency percentage (%ME) is the response. CCD which is the most frequently used five-level fractional design is employed here for experimental design and construction of response surface model. We aim to demonstrate how the operating parameters influence the process performance. The mineralization kinetic during the process is also investigated.

2. Materials and methods

2.1 Materials

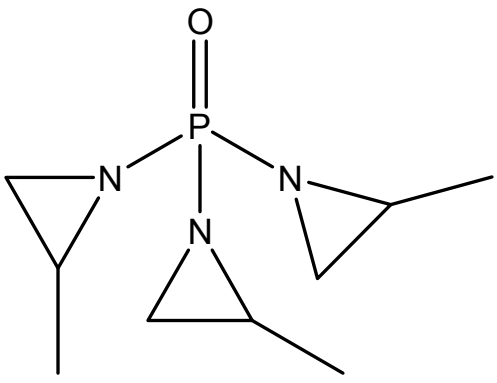

Fig. 1 The structure of MAPO molecule

MAPO ($C_9H_{18}N_3OP$, MW = 215.23 g mol^{-1}), (Fig. 1) was synthesized according to the method introduced by Kawamoto and Wills (2002). Nano titanium dioxide, PlasmaChem GmbH, P25 (80% anatase, 20% rutile, size 21 ± 10 nm and surface area 50 m^2 g^{-1}) grade with purity more than 99.5% was used as photocatalyst. Sulfuric acid and sodium hydroxide (to adjust pH) were purchased from Merck.

2.2 Photo-reactor and procedure

A 3.3 L stainless steel photo-reactor was designed and used. Fig. 2 demonstrates the schematic view of this photo-reactor and its fittings. The light source was mercury 250 W UV lamp (280-400 nm), located horizontally in a quartz tube at the center of the reactor. The maximum emission (348 $mWcm^{-2}$) was at 365 nm, measured by a TOPCON UV-R-1 spectroradiometer. The reactor was equipped with a stainless steel water-flow coil, containing an external circulating flow of a thermostat bath (OPTIMA-740, Japan) which could adjust temperature with an accuracy of ± 0.1°C.

Owing to light intensity decrease with distance from a lamp, positioned above the liquid content level or immersed in the solution bulk; only a small part of the reaction medium is effectively utilized, just around the light source (Eltayeb *et al*. 2010). Meanwhile, the substrate undergoes a degradation reaction in which intermediates can be produced and remain for long times (Levenspeil 1999). Therefore, in this reactor, the content was circulated and sprayed over the quartz tube, so that a falling film was formed around it. This device has the advantage of direct irradiation for the aim of substrate mineralization via sequential reactions. After envisaging direct light by the falling film, it enters the bulk content, just below the falling zone; while the transmission photons can still be received. All inside reactor sides, including top removable

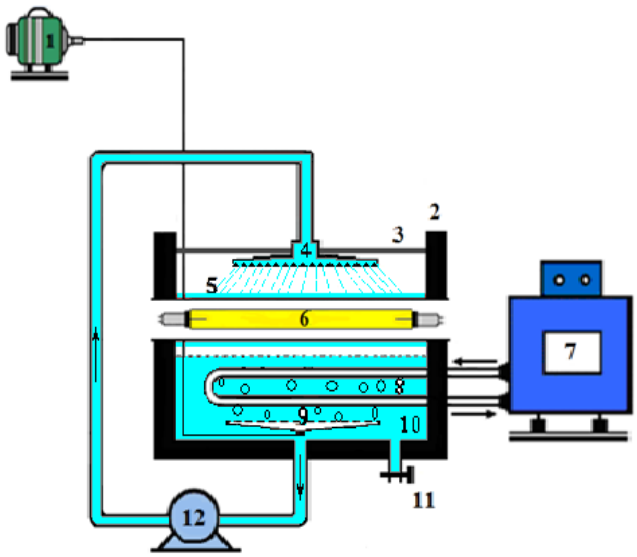

Fig. 2 The schematic view of the photo-reactor set up. 1: micro air compressor, 2: reactor wall, 3: aluminum foil, 4: liquid distributor, 5: quartz tube, 6: UV lamp, 7: thermostat, 8: water-flow coil, 9: air distributor, 10: MAPO solution, 11: drain valve, 12: circulating pump

head, were made of stainless steel and were reflective. For estimated supplying incumbent oxygen of photocatalytic process; air bubbles were generated by micro-air compressor via a distributor.

To perform the experiments, the appropriate solutions containing a known amount of MAPO and suspended TiO_2 particles were first prepared and sonicated to homogenize the nano particles throughout the solution. The pH was adjusted to a desired value by means of a pH meter (Denver, UB-10) using a dilute H_2SO_4 or NaOH solution. The solution was transferred to the reactor and then temperature was adjusted. Samples (5 mL) for analysis were taken at the beginning and the end of experiments (after 120 min), then thoroughly centrifuged to separate TiO_2 nano particles. The lamp was switched on 5 min prior to experiments for reaching steady state irradiation.

2.3 Sample analysis

The progress of photocatalytic mineralization of the substrate was followed by measuring the chemical oxygen demand (COD) of samples. COD values have been related to the total concentration of organics in the solutions (Daneshvar *et al*. 2005, Saien *et al*. 2011) and measurements were based on standard closed reflux method (APHA 1998) by means of a digital COD reactor (HACH, DRB 200). In each case, 2 mL of samples was added to a COD vial and then were refluxed at 150˚C for 120 min. After cooling, COD of each sample was measured using corresponding spectrophotometer (HACH, DR 2800). The percentage of mineralization efficiency can be defined as

$$\%\mathrm{ME} = \frac{\mathrm{COD}_0 - \mathrm{COD}_\mathrm{f}}{\mathrm{COD}_0} \tag{1}$$

where COD_0 and COD_f are the initial and final chemical oxygen demand of the solutions, respectively.

2.4 Experimental design strategy

The most popular case of RSM design is CCD. The total number of design points (experimental runs) in a CCD can be formulated as $N = 2^k + 2k + N_0$ (Khuri and Mukhopadhyay 2010), where k is the number of factors, 2^k is the cubic runs, $2k$ is the axial runs and N_0 is the center point runs. The center point of CCD is used to calculate the experimental errors. The distance of the axial points from the center point depend on the number of factors (Montgomery 2001). Accordingly, nano TiO_2 dosage (A), initial pH (B), temperature (C) and MAPO initial concentration (D) were independent variables and %ME, as a performance index, is the response. Each variable in the design was examined at five different levels ($-\alpha$, −1, 0, 1, $+\alpha$). All variables were taken at a central coded value considered to be zero. Table 1 lists the levels of the used variables. The ranges of these variables were chosen considering a number of preliminarily experiments and the previous relevant experimental results (Saien and Soleymani 2009). The distance of the axial points from the center point is named α (alpha) (Sakkas and Islam 2010). In this study, coded α value was fixed at 2 and actual value of α can be determined by the multiplication fixed coded α value with the step of factor level and then summation or subtraction of obtained value from the central point. For example, the center point value of MAPO initial concentration is 50 mg L^{-1} and the step of factor level is 10 mg L^{-1} ; so, $-\alpha$ will be $50 - (10 \times 2)$ and $+\alpha$ will be $50 + (10 \times 2)$. The applied CCD was consisted of 30 experimental runs ($N = 2^4 + 4 \times 2 + 6 = 30$) for which the design matrix is depicted in Table 2.

Table 1 The used coded and actual levels of independent variables

Variable	Coded and actual levels				
	$-\alpha$	–1	0	+1	$+\alpha$
A: $[TiO_2]$, mg L^{-1}	0	50	100	150	200
B: pH	2.5	4.5	6.5	8.5	10.5
C: *T*, ˚C	15	20	25	30	35
D: $[MAPO]_0$, mg L^{-1}	30	40	50	60	70

Table 2 CCD experimental design matrix and results with actual and coded variable levels

Run	$[TiO_2]$, mg L^{-1}	Initial pH	*T*, ˚C	$[MAPO]_0$, mg L^{-1}	%ME
1	100 (0)	6.5 (0)	15 ($-\alpha$)	50 (0)	1.01
2	150 (+1)	4.5 (–1)	30 (+1)	60 (+1)	12.60
3	100 (0)	6.5 (0)	25 (0)	50 (0)	10.09
4	100 (0)	10.5 ($+\alpha$)	25 (0)	50 (0)	9.11
5	150 (+1)	8.5 (+1)	20 (–1)	60 (+1)	5.04
6	100 (0)	6.5 (0)	25 (0)	50 (0)	9.09
7	50 (–1)	8.5 (+1)	20 (–1)	40 (–1)	3.80
8	150 (+1)	8.5 (+1)	30 (+1)	40 (–1)	10.13
9	50 (–1)	4.5 (–1)	20 (–1)	40 (–1)	3.79
10	100 (0)	6.5 (0)	25 (0)	50 (0)	9.07
11	0 ($-\alpha$)	6.5 (0)	25 (0)	50 (0)	1.01
12	100 (0)	6.5 (0)	25 (0)	50 (0)	9.10
13	100 (0)	6.5 (0)	25 (0)	50 (0)	9.09
14	100 (0)	2.5 ($-\alpha$)	25 (0)	50 (0)	7.07
15	150 (+1)	8.5 (+1)	20 (–1)	40 (–1)	2.53
16	150 (+1)	8.5 (+1)	30 (+1)	60 (+1)	15.97
17	150 (+1)	4.5 (–1)	20 (–1)	40 (–1)	3.80
18	100 (0)	6.5 (0)	25 (0)	70 ($+\alpha$)	21.74
19	150 (+1)	4.5 (–1)	30 (+1)	40 (–1)	10.13
20	50 (–1)	8.5 (+1)	30 (+1)	60 (+1)	15.13
21	50 (–1)	8.5 (+1)	20 (–1)	60 (+1)	7.56
22	200 ($+\alpha$)	6.5 (0)	25 (0)	50 (0)	3.03
23	100 (0)	6.5 (0)	25 (0)	50 (0)	8.08
24	50 (–1)	8.5 (+1)	30 (+1)	40 (–1)	10.13
25	100 (0)	6.5 (0)	35 ($+\alpha$)	50 (0)	12.12
26	100 (0)	6.5 (0)	25 (0)	30 ($-\alpha$)	12.07
27	50 (–1)	4.5 (–1)	30 (+1)	60 (+1)	7.01
28	150 (+1)	4.5 (–1)	20 (–1)	60 (+1)	5.88
29	50 (–1)	4.5 (–1)	20 (–1)	60 (+1)	7.56
30	50 (–1)	4.5 (–1)	30 (+1)	40 (–1)	6.01

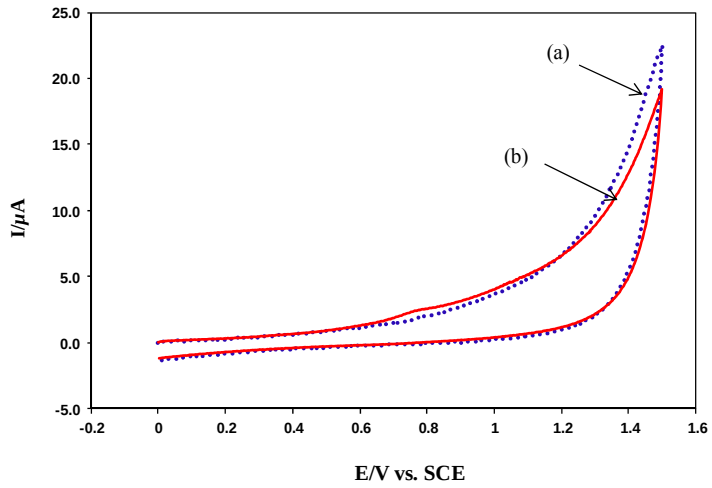

Fig. 3 Cyclic voltammograms of (a) phosphate buffer (0.2 M) (pH = 8.5) and (b) 1 mM of MAPO in the buffer; scan rate: 100 mV s^{-1} and $T = 25^{\circ}C$

3. Results and discussion

The mineralization range of MAPO is from 1.01% to 21.74% (see Table 2). This indicates that MAPO in aqueous solution is rather resistant to oxidation. In this regard, to evaluate the oxidation feasibility of the substrate, a Cyclic Voltammetric (CV) test was provided in aqueous solution with typical MAPO concentration of 10^{-3} mol L^{-1} (Arias-Pardilla *et al*. 2010) in phosphate buffer (0.2 mol L^{-1}) under pH = 8.5. The obtained voltammograms (Fig. 3) indicate that MAPO solution behaves very similar to just non-active oxidation phosphate buffer, and the appeared variations (mostly for $E > 1.2$ V) can be attributed to water oxidation (Nematollahi and Maleki 2009). A part of difficulty on MAPO mineralization can be due to nitrogen and phosphorous atoms in its molecular structure which are oxidized mostly to NO_3^- and PO_4^{3-} in the photocatalytic processes (Herrmann 1999). Several mechanisms for fouling effects of such inorganic ions on TiO_2 photo-activity have been proposed (Burns *et al*. 1999). These include competitive adsorption to surface active sites, radical and hole scavenging and direct reaction with the photocatalyst (Habibi *et al*. 2005, Hu *et al*. 2003).

3.1 Modeling the mineralization process

The step-wise model fitting by the Design Expert software (Trial version 8, Stat-Ease, Inc., MN) was used to determine the best mathematical expression for the percentage of mineralization. Based on the appropriate "lack-of-fit" (the variation between the model prediction and the experimental responses) and other model statistics criteria a quadratic model was selected, in the form

$$y_{\text{pred}} = \beta_0 + \sum_{i}^{k} \beta_i x_i + \sum_{i}^{k} \beta_{ii} x_i^2 + \sum_{i}^{k-1} \sum_{j=i+1}^{k} \beta_{ij} x_i x_j + \varepsilon \qquad (2)$$

where y_{pred} is the predicted dependent variable, x_i and x_j are the independent variables, β_0 is the constant coefficient, β_i, β_{ii} and β_{ij} are the coefficients for linear, quadratic and interaction terms, respectively; and ε is the error. This mathematical expression has already been used in many attempts for modeling the pollutants treatments (Coelho *et al*. 2011, Betianu *et al*. 2008, Guaracho *et al*. 2009, Ahmadi *et al*. 2005).

The significance of the model terms was evaluated based on the *F* probability Prob > *F* at the 95% confidence level. Parameters with Prob > *F* less than 0.05 are statistically significant. The insignificant quadratic and interaction terms (B^2, AD and CD) were rejected to improve the model and then an analysis of variance (ANOVA) was performed for a reduced model (Table 3). The statistical criteria of the reduced model showed a value of 0.9732 for the determination coefficient (R^2, goodness of model fitting with data) which implies that 97.32% of the variations are explained by the model. Adj-R^2 (modified R^2 that adjusts for the number of explanatory terms in the model) value of 0.9554 is very close to the corresponding R^2 value that indicates there is a good proportion between the number of model terms and samples size. Also, predicted R^2 (indicates how well the model predicts responses for new observations) of 0.9067 is in reasonable agreement with the Adj-R^2.

The provided mathematical reduced expression for modeling mineralization efficiency in terms of coded values of the factors and in the form of Eq. (2), was given as

$$\begin{aligned}\%ME = {} & 8.73 + 0.34\,A + 0.69\,B + 2.93\,C + 1.92\,D - 0.63\,AB \\ & + 0.95\,AC + 1.05\,BC + 0.47\,BD - 1.79\,A2 - 0.65\,C2 + 1.93\,D2\end{aligned} \quad (3)$$

According to Table 3, the values of Prob > *F* less than 0.0001 and the high *F*-value of 57.46 imply that this model is adequate The recent criterion is calculated by model mean square divided

Table 3 ANOVA and lack-of-fit test for response quadratic reduced model[a]

Source	Sum of squares	df	Mean square	*F*-Value	Prob > *F*	Remarks
Model	384.73	11	53.16	57.46	< 0.0001	Significant
A	2.84	1	2.84	3.07	0.0967	
B	11.57	1	11.57	12.50	0.0024	
C	205.46	1	205.46	222.10	< 0.0001	
D	88.25	1	88.15	95.40	< 0.0001	
AB	6.39	1	6.39	6.90	0.0171	
AC	14.33	1	14.33	15.49	0.0010	
BC	17.69	1	17.69	19.12	0.0004	
BD	3.56	1	3.56	3.85	0.0654	
A^2	89.51	1	89.51	96.76	< 0.0001	
C^2	11.89	1	11.89	12.85	0.0021	
D^2	104.62	1	105.62	113.09	< 0.0001	
Residual	16.85	18	0.93			
Lack-of-fit	14.63	13	1.13	2.78	0.1329	
Pure error	2.02	5	0.40			
Cor total	601.38	29				Not significant

[a] $R^2 = 0.9732$; Adj-$R^2 = 0.9554$; pred-$R^2 = 0.9067$

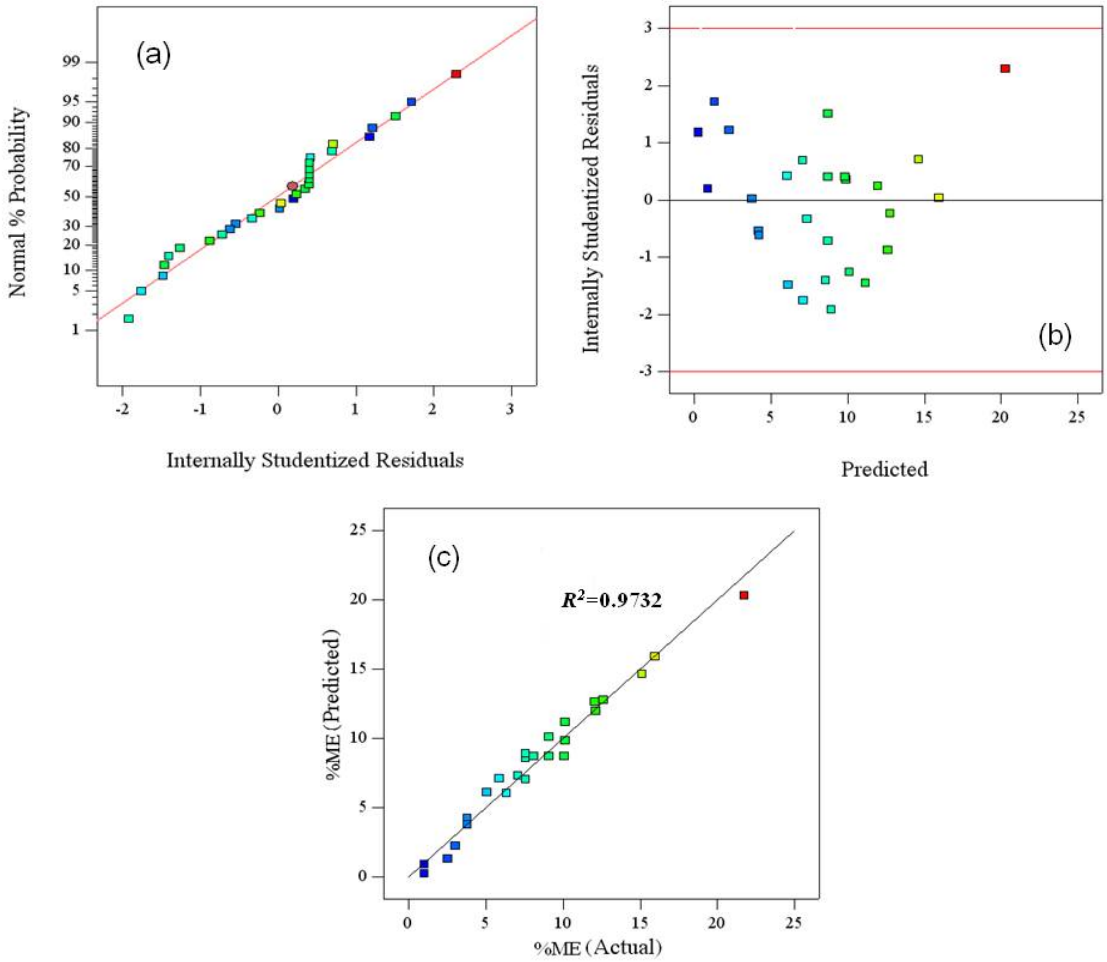

Fig. 4 (a) Diagnostic of the model: the normal probability residuals; (b) predicted mineralization efficiency percentage vs. studentized residuals, (c) plot of actual %ME vs. predicted %ME values

by residual mean square (Sakkas and Islam 2010). Also, the lack-of-fit *F*-value (test for comparing lack-of-fit variance with pure error variance) of 2.78 implies that the lack-of-fit is not significant relative to the pure error. There is a 13.29% chance that such lack-of-fit *F*-value could occur due to noise.

Important information about the model performance, other than those mentioned above, can be found in the diagnostic plots (Fig. 4), giving a concept of the agreement between the model fitting and the experimentally obtained data. The residuals (difference between the observed and the predicted response values) were analyzed using two graphical presentations: the plot of internally studentized residuals (The residual divided by the estimated standard deviation of that residual) vs. normal probability, and a plot of the predicted values vs. the internally studentized residuals. Points and points' clusters in the normal probability plot were placed very close to the diagonal line (Fig. 4(a)), indicating that (i) the errors were normally distributed and were independent from each other, (ii) the error variances are homogeneous and (iii) the residuals are independent from

each other (Dopar *et al*. 2010). The predicted values were plotted as a function of the internally studentized residuals to test the assumption of constant variance (Fig. 4(b)). Here, the points were scattered randomly and all values lie within the range of –3 to +3 which are considered as the top and bottom outlier detection limits (Sakkas and Islam 2010). In addition, a graphical representation of the actual vs. predicted values, (Fig. 4(c)), showed perfect model ability in reproducibility of the experimental data in the studied range.

A sensitivity analysis on the overall trend of mineralization variation under optimum conditions with the four considered variables (for each variable, others were constant), within the applied relevant ranges, showed that the mineralization process was strongly influenced by initial pH, followed by temperature, then MAPO initial concentration and finally nano TiO_2 dosage.

3.2 Validation of the model upon parameters' variation

The chemical and physical aspects of influencing variables were investigated. The model generated three dimensions and contour plots illustrate the kind of variations. In each plot two variables were kept constant (at the related zero levels) and the variation of %ME was depicted versus the two other variables, within the used ranges.

Fig. 5 shows the influence of initial pH and nano TiO_2 dosage on the mineralization. %ME increases with increase in the amount of the nano particles up to 110 mg L^{-1} and then decreases. In total, adding nano TiO_2 particles causes two different effects: (i) increasing active catalyst surface which leads to generation of more active species in the media (hydroxyl radical) and improving degradation efficiency, and (ii) increasing the media turbidity which leads to a decrease in the amount of lights to the catalyst surface and hence, diminishing the degradation efficiency. These opposite effects provide an optimum amount for the catalyst dosage. When the amount of nano

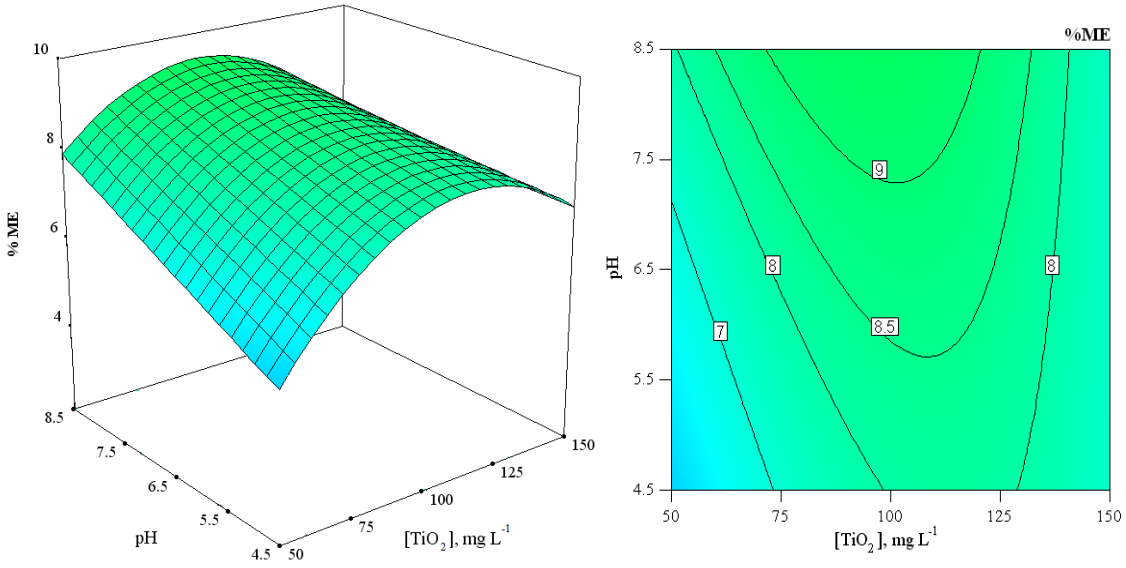

Fig. 5 The response surface and contour plots of the mineralization efficiency percentage versus TiO_2 dosage and initial pH; $[MAPO]_0$ = 50 mg L^{-1} ; T = 25˚C

TiO_2 particles increases, the solution turbidity is raised and the excess TiO_2 particles can create a light scattering effect that reduces the surface area of the photocatalyst being exposed to light illumination and consequently, the photocatalytic efficiency is decreased. In general, this phenomenon is called as "inner filtration effect" in photocatalysis (Serpone 1997, Guimarães and Barretto 2003). Further experiments under dark condition and in the presence of the nano TiO_2 particles showed no change in solution concentration, i.e., no degradation of MAPO molecules was occurred in this case. Also, as is relevant for run 11, no mineralization was observed in the case of lack of TiO_2.

pH is one of the important operational parameters affecting the rate of organic compounds degradation in a photocatalytic process. Fig. 5 also shows significant increase in %ME from acidic to alkaline pHs which can be attributed to the abundance of hydroxyl ions in the alkaline media, leading to easily generation of hydroxyl radicals with the aid of the valance band holes in nano TiO_2 particles (Saien and Soleymani 2007), compared with acidic media. It is notable that a 50 mg/L solution of MAPO provides a pH of about 6.5.

Interaction of pH and nano TiO_2 dosage on %ME can also be observed in Fig. 5. Dependency to pH is different at low and high amounts of nano TiO_2 particles. When catalyst dosage is low, the irradiated light is absorbed by the particles surface and sufficient oxidizing species are created. Under these conditions, availability of hydroxyl ions can play a positive role in producing more hydroxyl radicals. It is while, in the presence of higher amounts of nano TiO_2 particles, the particles due to turbidity will hinder the approach of the light to the catalysts surface. Hence, under the conditions that penetration of the light into the media has been limited; abundance of hydroxyl ions is not important. In this regard significance of pH and TiO_2 interaction term (AB) is stated by prob > *F* value of 0.0171 in Table 3.

The effects of temperature and nano TiO_2 dosage on the mineralization are shown in Fig. 6.

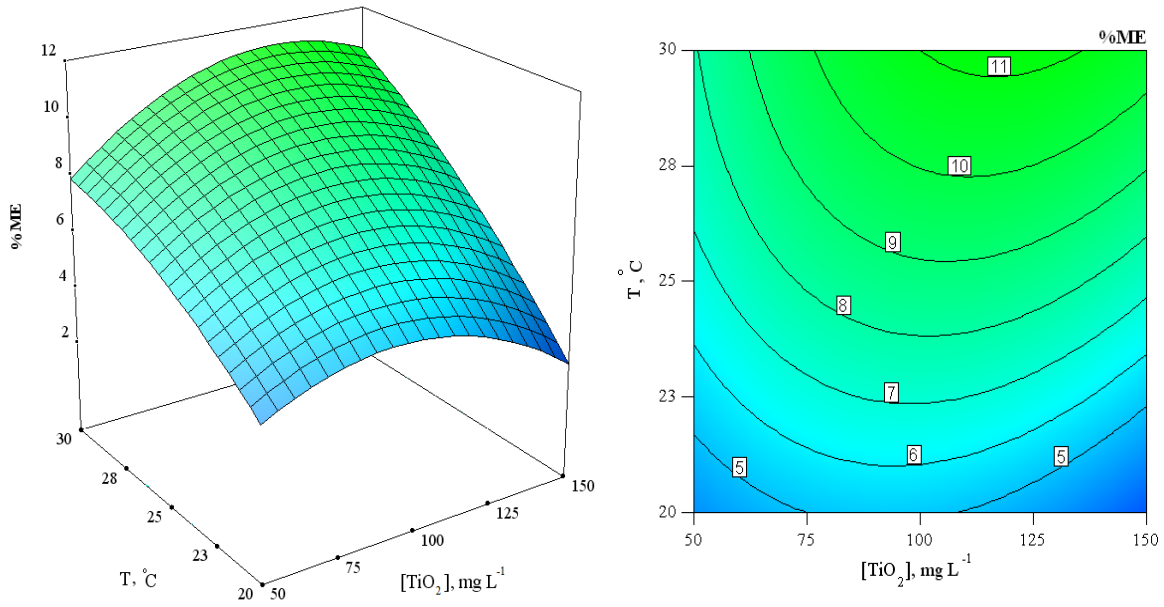

Fig. 6 The response surface and contour plots of the mineralization efficiency percentage as a function of the TiO_2 dosage and temperature; $[MAPO]_0$ = 50 mg L^{-1} and initial pH = 6.5

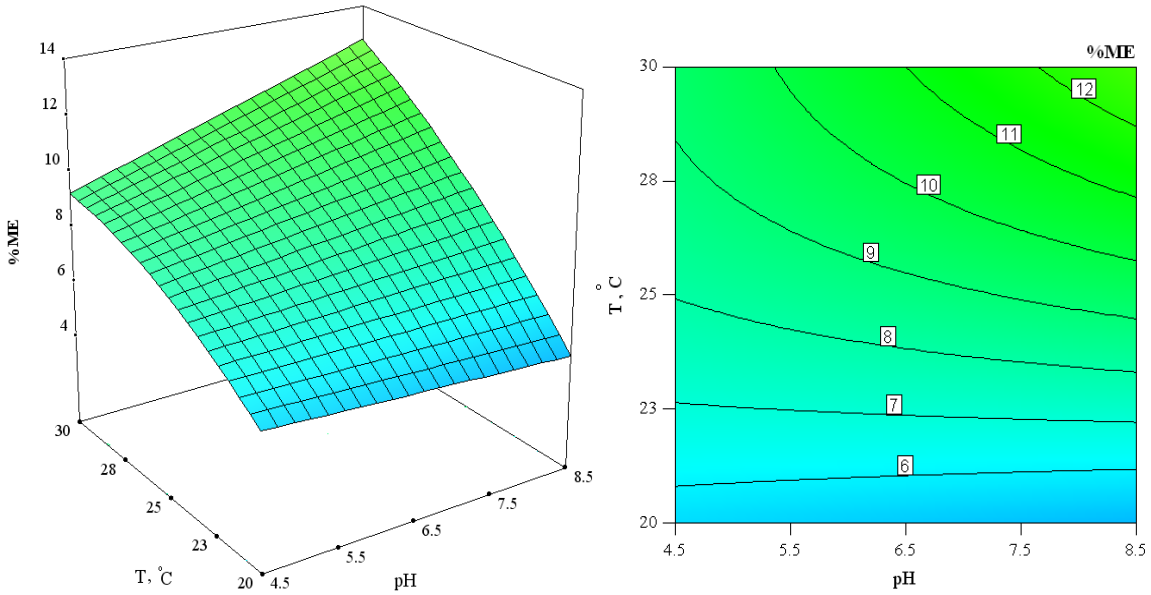

Fig. 7 The response surface and contour plots of the mineralization efficiency percentage as a function of initial pH and temperature; $[MAPO]_0$ = 50 mg L^{-1} and $[TiO_2]$ = 100 mg L^{-1}

Mineralization increases with temperature of the reaction media. This is due to overcoming the activation energy barriers belonging to the photocatalytic steps of hydroxyl radical generation and oxidative reaction of this species with the organics during treatment process. As this figure shows, there is an interaction between temperature and the amount of nano TiO_2 particles. The increase in temperature at high dosage of nano TiO_2 on mineralization is more effective rather than at low dosages (50 mg L^{-1} for instance). With low TiO_2 dosage, more incident photons will reach the unit of the catalyst surface, compared to the case of high TiO_2 dosage (which turbidity in the media is high) and therefore, more excitons (electron-hole) will be generated. Also, it has been found that recombination of excitons on the surface of photocatalysts will be promoted by temperature enhancement (Saien *et al*. 2010). This recombination due to temperature will be more extensive when excitons population on the catalyst surface is high (with low TiO_2 dosage). The importance of this interaction is reflected in Table 3 by the value of prob > *F* of 0.0010 for the term of AC.

Fig. 7 shows that temperature has important role in the process. At low and high temperatures, the effect of pH on mineralization efficiency was different. At low temperature, variation of pH has low effect, which means production of hydroxyl radicals is the limiting step. It is since producing hydroxyl radicals at low temperatures is not feasible and that presence of hydroxyl ions (in alkaline media) cannot promote it. As Table 2 shows, one of the lowest %ME values belongs to the run 1 in which temperature is at its lowest level of 15˚C. It is while at high temperatures, obtained %ME values clearly depend on the solution pH. Meanwhile, easier substrate mass transfer, at higher temperatures, can also accelerate the reaction. The BC prob > *F* of 0.0004 (Table 3) indicates the importance of temperature and pH interaction, as commented above.

Fig. 8 represents impact of initial pH and MAPO initial concentration interaction. The efficiency was enhanced when initial concentration of MAPO is increased. Several factors should be considered for this phenomenon. In general, mass transfer of the organic substrate in the liquid

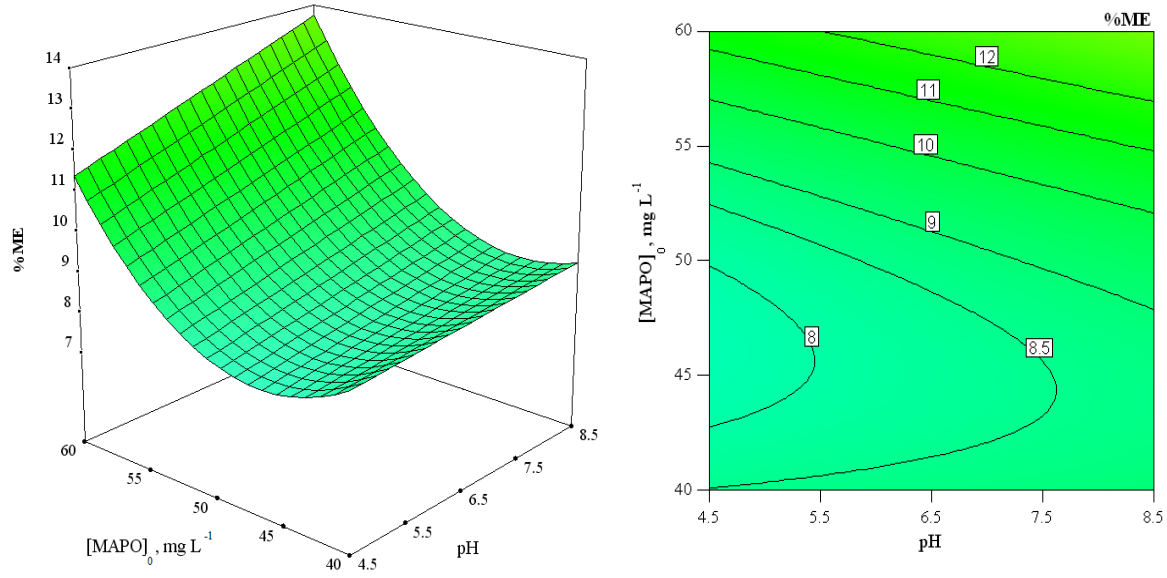

Fig. 8 The response surface and contour plots of the mineralization efficiency percentage as the function of initial pH and $[MAPO]_0$; $[TiO_2]$ = 100 mg L^{-1} and T = 25°C

phase to the catalyst surface is vital, and increasing the substrate content will help the substrate molecules to be accessible. On the other hand, since the lifetime of hydroxyl radicals is very short (only a few nanoseconds (Kasiri and Khataee 2011), they can only react where they are formed. Hence, increase in the number of MAPO molecules per solution volume unit will enhance the possibility of contact between the molecules and the hydroxyl radicals, leading to an increase in the treatment efficiency (Kasiri and Khataee 2011). It is notable that the amount of MAPO in solution does not have much effect on receiving light onto the surface of TiO_2 (there is no considerable UV light absorbance by MAPO). In addition, as shown in this figure, initial concentrations. It can be due to the ease of MAPO mass transfer toward the catalyst surface. When MAPO concentration is low, hence low amounts of substrate molecules are exposed to the surface of the TiO_2 particles; therefore, feasible producing of OH radicals in alkaline media cannot markedly affect the mineralization. However, with high MAPO concentrations, easier mass transfer will be exist and pH variation plays more effective role in the mineralization process. In this regard, prob > F of 0.0654 which is less than 0.1 and more than 0.05, for BD term in the Table 3 represents this minor interaction.

3.3 Process optimization

After screening the factors and their interactions, response surface analysis was used. Based on the desirability function (Sakkas and Islam 2010), the optimal conditions for the mineralization of MAPO was determined. The numerical optimization option of the software was used to introduce the specific point with the maximum desirability. The main objective was to maximize the %ME by recalculating all responsible factors using the desirability function. The goals for all variables were set “in the range”. By using described settings and boundaries, the software predicted 17.12%

for %ME under the optimized model factors of: 110 mg L^{-1} of TiO_2, T = 30°C, pH of 8.5 and MAPO initial concentration of 60 mg L^{-1}. In order to test the reliability, a further confirmatory experiment was conducted using the optimum parameters and 16.11% efficiency was obtained. This close agreement with the optimization analysis indicated that the developed model was robust and insensitive to external noise or tolerances by changing the factor levels.

3.3 Kinetic study

The kinetic of the photocatalytic mineralization was investigated under the optimum found conditions. A power law equation, based on chemical oxygen demand variation was applied as

$$r_m = -\frac{\mathrm{d\,COD}}{\mathrm{d}t} = k\,\mathrm{COD}^n \tag{4}$$

where r_m, k and n are the mineralization rate, the rate constant and the reaction order respectively. To obtain the appropriate parameters, the differential analysis method (Saien *et al*. 2011, Saien and Soleymani 2012) was used based on the data of COD amounts at different times (7 data points of COD values at different times until 150 min). From Eq. (4), the following equation is derived

$$\log r_m = \log k + n \log \mathrm{COD} \tag{5}$$

Fig. 9 presents the goodness of fitting the experimental data with this equation. Therefore; the following kinetic model was introduced for the rate of mineralization

$$r_m\left(\mathrm{mg\,O_2 L^{-1}.min^{-1}}\right) = 5.64\times10^{-6}\left(\left(\mathrm{mg\,O_2 L^{-1}}\right)^{-1.6}\mathrm{min^{-1}}\right)\mathrm{COD}^{2.6} \tag{6}$$

Several kinetic studies in photocatalytic process have been presented with power law models (Kumar *et al*. 2007, Saien *et al*. 2003). The reaction order of 2.6 indicates a complex reaction mechanism.

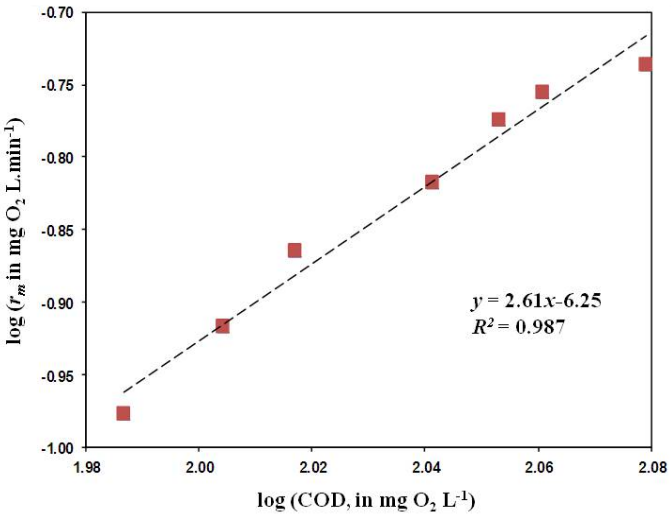

Fig. 9 Kinetic plot of the variation of log r_m vs. log (COD)

4. Conclusions

In this study, the photocatalytic mineralization of MAPO in aqueous solutions was investigated. A falling film photo-reactor was utilized with suspended nano TiO_2 photocatalytic particles. Accordingly, response surface methodology was used for the experimental designs and modeling. The following specific conclusions can be drawn: (i) despite a stable MAPO structure in aqueous solution, a considerable mineralization efficiency, within considered operating ranges, can be achieved after 120 min; (ii) response surface methodology is efficient for optimization of the process and a reduced quadratic mathematical expression can predict the process behavior well; (iii) the optimum conditions for the process was found as: $[TiO_2]$ = 110 mg L^{-1}, initial pH of 8.5, T = 30˚C and $[MAPO]_0$ = 60 mg L^{-1}; (iv) the impact of the applied factors on the mineralization efficiency around the optimum conditions is in the order of: initial pH > temperature > MAPO initial concentration > TiO_2 dosage; and (v) a power law equation based on COD with an order of 2.6 describes the mineralization kinetic, under optimum conditions until 150 min of the process progress.

Acknowledgements

The authors would like to thank the university authorities for providing the financial support to carry out this work.

References

Ahmadi, M., Vahabzadeh, F., Bonakdarpour, B., Mofarrah, E. and Mehranian, M. (2005), "Application of the central composite design and response surface methodology to the advanced treatment of olive oil processing wastewater Fentons peroxide", *J. Hazard. Mater.*, **123**(1-3), 187-195.

Arias-Pardilla, J., Otero, T.F., Blanco, R. and Segura, J.L. (2010), "Synthesis, electropolymerization and oxidation kinetics of an anthraquinone-functionalized poly (3,4-ethylenedioxythiophene)", *Electrochim. Acta*, **55**(5), 1535-1542.

APHA (1998), *Standard Methods for the Examination of Water and Wastewater*, 20th Edition, Washington DC.

Betianu, C., Caliman, F.A., Gavrilescu, M., Cretescu, I., Cojocaru, C. and Poulios, I. (2008) "Response surface methodology applied for Orange II photocatalytic degradation in TiO_2 aqueous suspensions", *J. Chem. Technol. Biot.*, **83**(11), 1454-1456.

Burns, R.A., Crittenden, J.C., Hand, D.W., Selzer, V.H., Sutter, L.L., Salman, S.R. (1999), "Effect of inorganic ions in heterogeneous photocatalysis of TCE", *J. Environ. Eng.*: *ASCE*, **125**(1), 77-85.

Coelho, L.F., de Lima, C.J.B., Rodovalho, C.M., Bernardo, M.P. and Contiero, J. (2011), "Lactic acid production by new Lactobacillus plantarum LMISM6 grown in molasses: optimization of medium composition", *Braz. J. Chem. Eng.*, **28**(1), 27-36.

Daneshvar, N., Rabbani, M., Modirshahla, N. and Behnajady, M.A. (2005), "Photooxidative degradation of Acid Red 27 in a tubular continuous-flow photoreactor: Influence of operational parameters and mineralization products", *J. Hazard. Mater.* **118**(1-3), 155-160.

Dopar, M., Kusic, H. and Koprivanac, N. (2010), "Treatment of simulated industrial wastewater by photo-Fenton process. Part I: The optimization of process parameters using design of experiments (DOE)", *Chem. Eng. J.*, **173**(2), 267-279.

Eltayeb, A.E., Khalil, O., Alhallaj, S. and Teymour, F. (2010), "Design and modeling of optimization of optical modules for use in the "Emerald Forest" algae photobioreactors", *Comput. Chem. Eng.*, **34**(9),

1323-1340.
Gembitskii, P.A., Loim, N.M. and Zhuk, D.S. (1966), "Aziridine: Synthesis, structure, properties", *Russ*. *J*. *Chem*. *Rev*., **35**(2), 105-122.
Guaracho, V.V., Kaminari, N.M.S., Ponte, M.J.J.S. and Ponte, H.A. (2009), "Central composite experimental design applied to removal of lead and nickel from sand", *J*. *Hazard*. *Mater*., **172**(2-3), 1087-1092.
Guimarães, J.R. and Barretto, A.S. (2003), "Photocatalytic inactivation of Clostridium perfringens and coliphages in water", *Braz*. *J*. *Chem*. *Eng*., **20**(4), 403-411.
Habibi, M.H., Hassanzadeh, A. and Mahdavi, S. (2005), "The effect of operational parameters on the photocatalytic degradation of three textile azo dyes in aqueous TiO_2 suspensions", *J*. *Photochem*. *Photobiol*. *A*: *Chem*., **172**(1), 89-96.
Herrmann, J.M. (1999), "Heterogeneous photocatalysis: fundamentals and applications to the removal of various types of aqueous pollutants", *Catal*. *Today*, **53**(1), 115-129.
Hu, C., Yu, J.C., Hao, Z. and Wong, P. (2003), "Effects of acidity and inorganic ions on the photocatalytic degradation of different azo dyes", *Appl*. *Catal*. *B*: *Environ*., **46**(1), 35-47.
Kabra, K., Chaudhary, R., and Sawhney, R.L. (2004), "Treatment of hazardous organic and Inorganic compounds through aqueous-phase photocatalysis: A review", *Ind*. *Eng*. *Chem*. *Res*., **43**(24), 7683-7696.
Kasiri, M.B. and Khataee, A.R. (2011), "Photooxidative decolorization of two organic dyes with different chemical structures by UV/H2O2 process: Experimental design", *Desalination*, **270**(1-3), 151-159.
Kawamoto, A.M. and Wills, M. (2002), "Enantioselective synthesis of aziridines using asymmetric transfer hydrogenation as a precursor for chiral derivatives used as bonding agent for rocket solid propellants", *Quím*. *Nova*, **25**(6A), 921-925.
Khuri, A.I. and Mukhopadhyay, S. (2010), "Response surface methodology", *Wiley Interdis*. *Rev*.: *Comput*. *Statis*., **2**(2), 128-149.
Kumar, K.V., Porkodi, K. and Selvaganapathi, A. (2007), "Constrain in solving Langmuir–Hinshelwood kinetic expression for the photocatalytic degradation of Auramine O aqueous solutions by ZnO catalyst", *Dyes Pigments*, **75**(1), 246–249.
Langsjoen, A., Jones, G.D., Zomlefer, J. and Neumann, N.M.C. (1944), "Polymerization of ethyleneimine", *J*. *Org*. *Chem*., **9**, 125-147.
Levenspiel, O. (1999), *Chemical Reaction Engineering*, 3rd Edition, John Wiley and Sons, NJ.
Montgomery, D.C. (2001), *Design and Analysis of Experiments*, 5th Edition, John Wiley and Sons, NJ.
Nematollahi, D. and Maleki, A. (2009) "Electrochemical oxidation of *N*,*N*-dialkyl-*p*-phenylenediamines in the presence of arylsulfinic acids. An efficient method for the synthesis of new sulfonamide derivatives", *Electrochem*. *Commun*., **11**(2), 488-491.
Parsa, J.B. and Abbasi, M. (2010), "Modeling and optimizing of sonochemical degradation of Basic Blue 41 via response surface methodology", *Cent*. *Eur*. *J*. *Chem*., **8**(5), 1069-1077.
Saien, J., Ardjmand, R.R. and Iloukhani, H. (2003), "Photocatalytic decomposition of sodium dodecyl benzene sulfonate under aqueous media in the presence of TiO_2", *Phys*. *Chem*. *Liq*., **41**(5), 519-531.
Saien, J., Delavari, H. and Solymani, A.R. (2010), "Sono-assisted photocatalytic degradation of styrene-acrylic acid copolymer in aqueous media with nano titania particles and kinetic studies", *J*. *Hazard*. *Mater*., **177**(1-3), 1031-1038.
Saien, J., Ojaghloo, Z., Soleymani, A.R. and Rasoulifard, M.H. (2011), "Homogeneous and hetrogeneous AOPs for rapid degradation of Triton X-100 in aqueous media via UV light, nano titania, hydrogen peroxide and potassium persulfate", *Chem*. *Eng*. *J*., **167**(1), 172-182.
Saien, J. and Soleymani, A. (2007), "Degradation and mineralization of Direct Blue 71 in a circulating upflow reactor by UV/TiO_2 process and employing a new method in kinetic study", *J*. *Hazard*. *Mater*., **144**(1-2), 506-512.
Saien, J. and Soleymani, A.R. (2009), "Comparative investigations on nano and micro titania photocatalysts in degradation and mineralization: Use of turbidity in kinetic studies", *J*. *Iran Chem*. Soc., **6**(3), 602-611.
Saien, J. and Soleymani, A.R. (2012), "Feasibility of using a slurry falling film photo-reactor for individual and hybridized AOPS", *J*. *Ind*. *Eng*. *Chem*. **18**(5), 1683-1688.
Sakkas, V.A., Islam, M., Stalikas, C. and Albanis, T.A. (2010), "Photocatalytic degradation using design of

experiments: A review and example of the Congo red degradation", *J. Hazard. Mater.*, **175**(1-3), 33-44.
Serpone, N. (1997), "Relative photonic efficiencies and quantum yields in heterogeneous photocatalysis", *J. Photochem. Photobiol. A: Chem.*, **104**(1-3), 1-12.
Thiruvenkatachari, R. Vigneswaran S. and Moon I.S. (2008), "A review on UV/TiO_2 photocatalytic oxidation process", *Korean J. Chem. Eng.*, **25**(1), 64-72.